

Polariton pulse propagation through GaAs: Excitation-dependent phase shifts

J. S. Nägerl, B. Stabenau, G. Böhne, S. Dreher, and R. G. Ulbrich
IV. Physikalisches Institut der Universität Göttingen, Bunsenstr. 13, Göttingen, Germany

G. Manzke* and K. Henneberger
Universität Rostock, Fachbereich Physik, Universitätsplatz 3, D-18051 Rostock, Germany
 (Received 24 August 2000; published 18 May 2001)

We report on amplitude and phase measurements of ultrashort laser pulses after propagation through a 3.8 μm thick GaAs platelet at 2 K. The incident center frequency of the 40 fs, 1.525 eV pulses was tuned slightly above the fundamental gap energy. Apart from intensity beats due to polariton propagation we find characteristic phase shifts in the transmitted optical field and investigate their dependence on excitation density. For low excitation [$< 10^{13}$ electron-hole ($e-h$) pairs/cm 3] a phase jump of $+\pi$ occurs at each individual beat node. With increasing excitation (up to 10^{15} $e-h$ pairs/cm 3) these jumps flip successively from $+\pi$ to $-\pi$. A simple Lorentzian oscillator model for the dielectric function fails to describe this effect, which is shown to be caused by density-dependent asymmetries and shifts of the exciton lines. A thorough theoretical analysis of the edge spectrum based on semiconductor Bloch equations (SBE) shows that the asymmetries are due to many-body effects. The standard SBE treatment is extended by including dephasing and renormalization of the interband energies in both wave number and frequency. The frequency dependence of these many-body effects is due to non-Markovian memory effects in the scattering term of the SBE. We find very good agreement with experiment in line shape and phase shift behavior for a wide range of pair densities.

DOI: 10.1103/PhysRevB.63.235202

PACS number(s): 71.35.Cc, 71.36.+c, 71.45.Gm

I. INTRODUCTION

The dielectric response of semiconductors for frequencies close to the fundamental gap is dominated by electron-hole ($e-h$) correlation. To lowest order in density, electrons and holes form excitonic pair states. For materials with a direct gap the interaction between light and the semiconductor is usually described in the framework of mixed exciton-photon excitations, so-called polaritons.¹ The excitonic polariton concept was outlined in a series of theoretical papers,^{2,3} and this pioneering work has inspired a considerable body of research on various spectral and transport properties of such systems.⁴ These studies revealed a complex behavior and a variety of linear and nonlinear effects in reflectance, emission, and light scattering spectra of bulk and layered semiconductors.^{5,6} The coherent propagation of excitonic polaritons through thin semiconductor platelets gave rise to qualitatively new phenomena: Fabry-Perot type resonances,⁷ slowing down of picosecond-pulse propagation near resonance,⁸ soliton-like transport,⁹ characteristic propagation beatings in transmitted intensity,¹⁰ and their dependence on parameters such as temperature¹¹ or excitation density^{12,13,15} were studied and analyzed in detail. Recently,¹⁴ effects of the spatial dispersion of polaritons in the linear absorption and phase spectra of bulk GaAs were examined.

In the regime of linear response, the polariton scheme reproduces the dielectric response of a dense ensemble of Lorentz oscillators that are weakly coupled to the electromagnetic field. Derivation of the linear dielectric response function is based on the self-consistent treatment of the dielectric polarization and the macroscopic electric field in Maxwell's equations. With increasing excitation the dielectric polarization is influenced by many-body effects between excited carriers. The Mott transition of excitons as a consequence of screening of the Coulomb interaction between car-

riers under conditions of increasing $e-h$ pair density is well understood. The effect of band-gap shrinkage and likewise reduction of exciton binding energies, leading to a nearly complete cancellation of two counteracting terms in the 1s exciton energy shift, was demonstrated in several experiments (see Ref. 16 for GaAs). While the spectral position of the lowest exciton stayed largely unchanged with increasing excitation density, the sharp line feature broadened and gradually disappeared in the structureless continuum spectrum of above-band-gap states. The solution of the wave equation of the Wannier exciton embedded in the equilibrium plasma of excited $e-h$ pairs gave indeed strong compensation of gap shrinkage and weakening of the Coulomb interaction due to dynamic screening.¹⁷ Later it became clear that the nonlinear excitonic behavior cannot be described with a simple static screening model;^{18,19} it would lead to a strong redshift of the exciton, which is not observed in experiments. Dynamical screening has to be taken into account, either within a plasmon-pole approximation¹⁷ or with a Lindhard dielectric function.²⁰⁻²² The problem of such an approach lies in the use of the Shindo approximation, which is applied to solve the Bethe-Salpeter equation for the polarization function including dynamical screening. The results turn out to be restricted to carrier densities well below the Mott transition, since divergencies appear if the sum of the carrier distribution functions goes to 1.

This problem can be avoided by using the semiconductor Bloch equations²³ (SBE). Now the many-body effects appear in the scattering terms of the kinetic equations for the two-band density matrix, and here the Markovian treatment of the scattering terms corresponds to the above-mentioned Shindo approximation. In the so-called dephasing rate approximation, collisions between carriers are assumed to be responsible for the so-called diagonal dephasing, while off-diagonal

dephasing is induced by carrier-polarization scattering. Both effects compensate one another and are contained in the imaginary parts of the retarded interband self energy and the effective electron-hole interaction. They represent many-body effects that go beyond the corresponding Hartree-Fock approximations.^{24,25} In earlier work^{26–28} the real parts of the retarded interband self-energy and the effective interaction had been approximated by a simple static screening model, which was later improved by full treatment of the real parts, the latter calculated via a Kramers-Kronig transformation of the imaginary parts.^{29–32} These approaches were altogether based on the Markovian treatment of scattering integrals. They correspond to Boltzmann-like scattering terms, used, e.g., in heuristic treatments of carrier-carrier scattering.

We demonstrate here that this simple approach fails to describe correctly the details of experimental high-resolution excitonic absorption spectra and especially their dependence on excitation conditions, i.e., the density and temperature of the e - h plasma in quasiequilibrium. Our treatment goes beyond the Markovian treatment of the scattering integrals and takes memory effects into account. After transforming from time-to-frequency domain they appear as strongly frequency dependent many-body effects in the region around the lowest exciton up to the band gap and also into the continuum. Signatures of non-Markovian memory effects were already reported in Refs. 33–38.

In earlier papers^{26–31} the dynamically screened potential in the scattering matrix element was approximated by its static limit. In comparison to treatments our theory takes fully into account the dynamical screening. In recent work²⁵ it has been demonstrated that the approach used here is also able to explain the peculiar temperature and density dependence of the $1s$ exciton energy in ZnSe. Here a weak blueshift at lower temperatures turns into a redshift above 30 K at fixed pair density. This approach corresponds to that in Refs. 36 and 37, where the buildup of dynamical screening and its influence on the time evolution of four-wave-mixing signals was demonstrated.

Application of our approach with the SBE to calculate the dielectric function of the semiconductor enables us to explain in detail the measured amplitude and phase behavior of polariton pulse propagation in terms of frequency-dependent many-body effects. In addition to the treatments in Refs. 25, 36, and 37 we also demonstrate here that it is important to take into account the renormalization of the energy and lifetime of carrier states contained in the formulation of the SBE. They are taken as broadened carrier spectral functions instead of simple δ -like functions peaked at the carrier dispersion.

The paper is organized as follows: Section II describes the Fourier spectroscopy setup, and Sec. III presents interferograms and their interpretation in the linear regime. In Sec. IV the latter interferograms are presented for the nonlinear case and compared with those of many-body theory.

II. EXPERIMENTAL METHOD

With our experimental setup we perform Fourier spectroscopy with a Mach-Zehnder interferometer, which is opti-

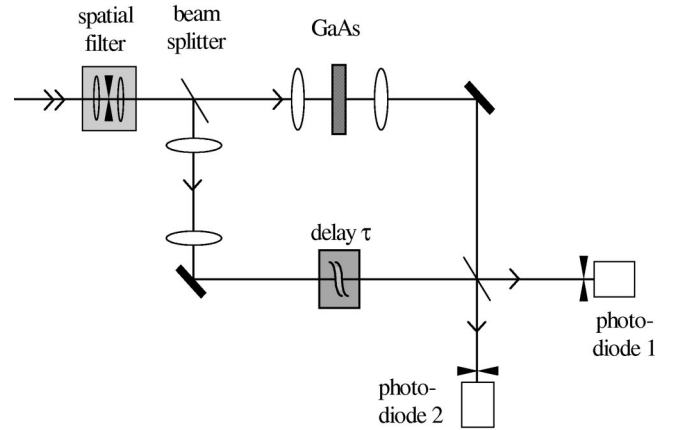


FIG. 1. Experimental setup of the interferometer: All three optical signals (i.e., sample/reference cross-correlation and Ti:sapphire and He-Ne autocorrelation) follow closely spaced paths to avoid spurious dispersion effects in the four-beam splitting and four focusing elements.

mized for the use of ultrashort laser pulses as an incident light source. A numerical algorithm on a personal computer (PC) is used for amplitude and phase retrieval from the measured interferograms, i.e., the cross-correlation and autocorrelation intensities. Three optical signals are measured simultaneously after transmission through the interferometer: (i) the cross-correlation intensity of 40 fs, 1.525 eV Ti:sapphire laser pulses, which contains all information on the optical response function of the sample, (ii) the autocorrelation intensity of the Ti:sapphire pulses as an online check of the central frequency of the incident laser pulses, and (iii) an auto-correlation of a cw He-Ne laser representing a stable oscillator (“wavemeter”) that calibrates the interferometer online. All three beams are detected in analog form, converted into digital signals with 16-bit analog-to-digital converters (ADC’s), and processed with a numerical lock-in algorithm using the He-Ne laser frequency as a reference. Mechanical noise and thermal drift of the setup are thus reduced considerably and an accuracy of approximately 1/30 fringe over a typically 10 ps range of the delay time τ at 1 Hz bandwidth is achieved.

The modulation of the interference signal behind the second beam splitter as a function of delay time τ is measured with two low-noise Si p - n detectors, each behind pinholes well adapted to the size and adjusted to the center fringe of the interference pattern (see Fig. 1). By subtracting the photodiode signals from each other and using a spatial filter in front of the interferometer, baseline intensity fluctuations and angular jitter of the laser are greatly reduced. The beam splitters are wedge shaped to avoid multiple reflections. The measured signal is proportional to the cross-correlation $C(\tau)$ of the signal pulse $E_{sig}(t)$ with the delayed reference pulse $E_{ref}(t + \tau)$:

$$C(\tau) \propto \int dt 2 E_{sig}(t) E_{ref}(t + \tau). \quad (1)$$

Its amplitude $E_0(\tau)$ and phase $\varphi(\tau)$ that are defined with $C(\tau) \equiv E_0(\tau) \cos[\omega_0 \tau + \varphi(\tau)]$ are retrieved by calculating the integral

$$\frac{\omega_0}{2\pi} \int_{\tau - \pi/\omega_0}^{\tau + \pi/\omega_0} d\tau' C(\tau') \exp(-\omega_0 \tau') \equiv \frac{1}{2} E_0(\tau) e^{i\varphi(\tau)}, \quad (2)$$

where the phase is taken relative to a reference phase which is chosen here to be the low-density 1s-exciton frequency $\omega_0 = 1.515$ eV. To achieve a high phase resolution it is important that all three beams follow closely similar optical paths passing through the same optical components. Dispersion effects of the interferometer are avoided by using a fully symmetric setup and are carefully checked with a spectrometer: tuning the delay around zero shows affine movements of all frequency components. We used nearly-chirp-free 40 fs pulses with the center frequency tuned to 1.525 eV from a Kerr-lens mode-locked Ti:sapphire laser at a repetition rate of 78 MHz that were characterized with standard techniques and gave chirp parameters $|\alpha| < 1.510^{-4} \text{ fs}^{-2}$, $|\beta| < 5.5 \times 10^{-6} \text{ fs}^{-3}$.

Our measurements cover a dynamic range of 3.5 orders of magnitude in the amplitude of the electric field at room temperature (being reduced to 3 orders at 2 K due to vibrations of the He cryostat pumps) and a phase resolution of up to 1/100 fringe in the center of the pulse. Time resolution in delay time $C(\tau)$ is limited in principle (i) by the dispersion of the interferometer, and (ii) in practice by the finite temporal width of 40 fs of the input (reference) pulses. Since very small average laser powers down to 10 fW can be detected in the linear interferometer setup, the Fourier spectroscopy method is suited to study phase shifts in optical spectra even at very low excitation densities.

The experiments were performed on a 3.8 μm thick, high-purity gallium arsenide platelet ($|N_d - N_a| < 2 \times 10^{14} \text{ cm}^{-3}$) grown by gas-phase epitaxy, held freely between glass plates and immersed in liquid He at 2 K. It had a linewidth [full width at half maximum (FWHM)] of the 1s resonance of $\hbar\gamma = 2 \times 50 \mu\text{eV}$ (for an optical density spectrum, see Fig. 2). We performed two variants of experiments: in the single-beam configuration the transmitted field was directly detected as a function of laser pulse fluence. In the two-beam configuration, a separate pump beam was focused on the sample, and we analyzed the weaker probe beam transmission as a function of the pump laser fluence and the delay time between the pump and the probe pulse.

III. LINEAR PULSE PROPAGATION

The behavior of the amplitude and the phase of the transmitted pulse at low mean excitation power $< 0.4 \text{ W/cm}^2$ is shown in Fig. 3. This excitation level represents the linear case: further reducing the laser pulse fluence did not change the measured spectra any more. It is evident from Fig. 3 that after propagation through the sample the 40 fs incident pulse is split into an aperiodic train of smooth maxima and minima with increasing beat period. This behavior is characteristic for polariton pulse propagation through a sufficiently thick

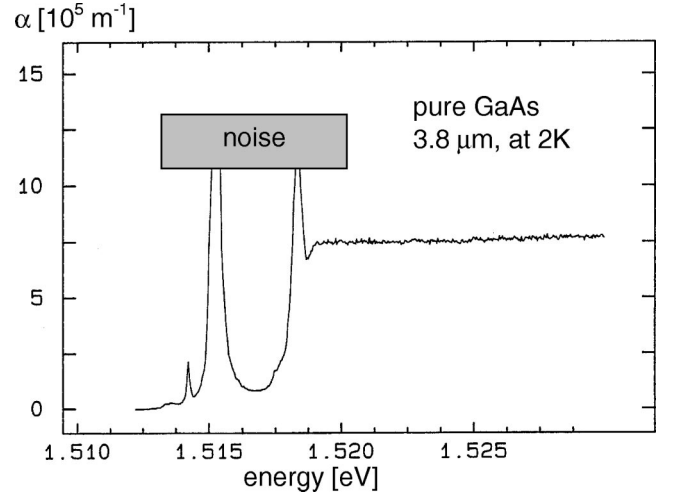


FIG. 2. Optical density spectrum of the sample taken with low-power cw incandescent white-light source. The height of the excitonic peaks is masked by detector noise and, for the 1s exciton, by luminescence.

plane-parallel slab.¹⁰ The beats are caused by interference of excitonic polaritons of the upper branch with those of the lower branch due to their phase and group velocity dispersion. From the positions of the minima we determine the oscillator strength of the 1s exciton resonance directly to be $86 \pm 5 \mu\text{eV}$. The beat nodes are accompanied by phase shifts close to π and have negative sign (i.e., point downwards in Fig. 3) for early $\tau = 0.7$ ps and late 7.8 ps delay time and point upwards (positive sign) for $\tau = 2.4$ and 4.3 ps. From the average slope of the phase signal trace we determine the momentary frequency of the total free polarization decay to be 1.515 eV, which agrees with the known low-density 1s-exciton resonance frequency in GaAs. The smooth extra modulation of the amplitude signal around 3 and 6 ps is caused by the interference of 1s- and 2s-exciton emission signals.

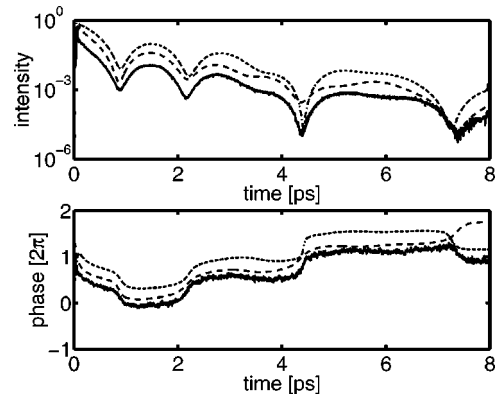


FIG. 3. Low-density limit for the squared amplitude (upper part) and the phase (lower part) of the measured transmitted electric field (solid line) together with results from simulations with a Lorentzian-broadened Elliot formula (3) (dashed) and a frequency-dependent non-Lorentzian damping (5) (dotted), see text. For better distinction with the experimental result both simulation curves are plotted with an offset.

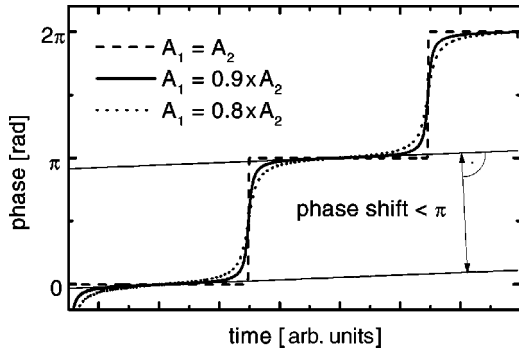


FIG. 4. Phase $\varphi(t)$ of the beating between two oscillations with $\omega_1 = 1.02\omega_2$.

Simulations using Fresnel's formulas without spatial dispersion show that for low excitation fair agreement with the experimental results, at least for τ in the range 0.5–7 ps can be found (see dashed line in Fig. 3), using a Lorentzian-broadened Elliot expression for the dielectric function³⁹ with damping of the successive excited exciton states γ_n (n is the principal quantum number⁴⁰) taken empirically as

$$\gamma_n = \gamma_{cont} + \frac{\gamma_1 - \gamma_{cont}}{n^2}, \quad (3)$$

with γ_1 being the damping rate for the $1s$ exciton and γ_{cont} the asymptotic rate for the continuum states. The analysis shows that the $2s$ exciton has a damping rate 5 times larger and the continuum states a damping rate 6 times larger than the lowest $1s$ exciton. A similar behavior was found in Ref. 41 for the $2s$ exciton through investigation of the pulse propagation in ZnSe-based microstructures.

However, there is no agreement with the measured phase in Fig. 3 at $\tau = 7.8$ ps: the experiment shows a negative phase jump $7.8ps$. In the simple broadened oscillator model the phase jumps for all τ are always positive. This indicates that the long-lived and strong $1s$ exciton resonance has a non-Lorentzian shape even in the low excitation regime.

In order to understand the meaning of the sign of a phase jump consider for simplicity the beating between two oscillators,

$$A_1 \cos(\omega_1 t) + A_2 \cos(\omega_2 t) = A(t) \cos[\omega_T t + \varphi(t)], \quad (4)$$

with two closely spaced frequencies $\omega_1 > \omega_2$ and amplitudes A_1 and A_2 . If $A_1 = A_2$ the phase of the superposition yields steplike phase shifts of $\pm\pi$ (see Fig. 4). If $A_1 > A_2$ ($A_1 < A_2$) the oscillation 1 (2) dominates and the phase jump $\varphi(t)$ of the superposition becomes smoother; the amount of the phase shift around the node is less than π and points upwards (downwards). Taking the limit $A_1 = 1$ and $A_2 = 0$ the phase is completely determined by oscillation 1 and shows no phase shift. Hence the sign of the phase shift is a very sensitive quantity to decide whether $A_1 > A_2$ or $A_1 < A_2$.

Obviously the signs of the phase shift are sensitive to the amplitudes of the two interfering wave packets on both polariton branches that arrive at the end of the sample at a

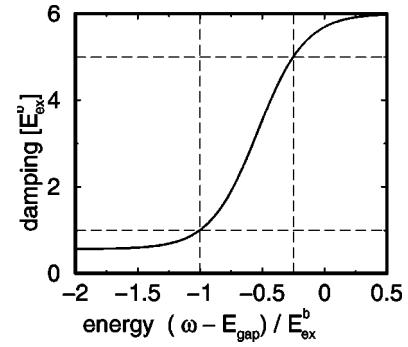


FIG. 5. Theoretical model for the damping of the nonexcited sample.

given time. Depending on initial amplitudes and eventual damping, either the upper or the lower polariton branch dominates and causes the phase jumps to have either positive or negative sign. In order to make the discrepancy between the simple model of broadened Lorentzian oscillators (3) and the experiment plausible (see Fig. 3), we model the damping ad hoc as an asymmetric function of the frequency

$$\gamma_0(\omega) = c_1 + c_2 \tanh(c_3 \omega + c_4) \quad (5)$$

in the region from the $1s$ exciton to the band gap. The parameters are chosen as follows: damping of the $1s$ state is taken to be $\gamma_0(E_{gap} - E_{ex}^b) = 50 \mu\text{eV}$ (E_{ex}^b is the excitonic Rydberg energy), the damping of the $2s$ state $\gamma_0(E_{gap} - E_{ex}^b/4) = 250 \mu\text{eV}$, as the limit high in the band $\gamma_0(\omega \gg E_{gap}) = 300 \mu\text{eV}$ (E_{gap} is the gap energy) is set, and the asymptotic $\gamma_0(\omega \ll E_{gap} - E_{ex}^b) = 28 \mu\text{eV}$ is fitted to get best agreement with the experiment. The overall shape of $\gamma_0(\omega)$ is shown in Fig. 5. In contrast to the expression (3), where one single damping constant is related to each exciton state γ_n and the continuum γ_{cont} , and where the dielectric function is a linear superposition of all these Lorentzian-like broadened resonances, Eq. (5) is now a smooth damping function in the frequency domain. Inserting it into the dielectric function based on the Elliot formula³⁹ gives phase and amplitude signals of the transmitted pulses that are presented in Fig. 3 with the dotted line. The phase at 7.8 ps now shifts downward, in agreement with the experiment. This points clearly at non-Lorentzian excitonic line shapes already at low excitation.

In Ref. 14 a shoulder on the high-energy side of the linear excitonic absorption was demonstrated to result from spatial dispersion effects. However, we find no influence of the effect of spatial dispersion on the behavior of the polariton beats in our much longer sample. Another possibility to explain the behavior of the phase could be an inhomogeneous distribution of pulse-excited carriers in the relatively long sample, since the absorption length of the sample (see Fig. 2) is about $1.3 \mu\text{m}$. Partitioning the sample into single slabs with a spatial inhomogeneous carrier distribution and Lorentzian-like dielectric functions could not explain the experimental findings. The resulting total absorption as an overlay of single Lorentzians becomes Lorentzian-like again. Only a strong blueshift of the exciton energy with increasing

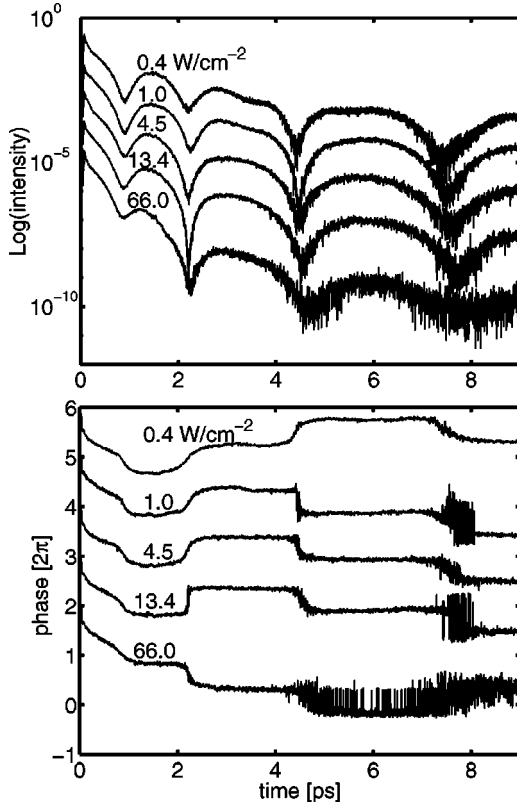


FIG. 6. Measured intensity and phase of the transmitted electric field (normalized) for different excitations (noise for higher fluences and at later times is caused by the rapidly vanishing amplitude in this case). For better distinction we have used a constant offset.

carrier density would generate an asymmetric absorption. However, the position of the exciton stays unchanged in the experiments. Since the experimental results also did not change qualitatively when we turned from one-beam to two-beam experiments we deduce that the analysis based on a spatially averaged carrier distribution is acceptable. There are other reasons for skewed line shapes of excitonic spectra, such as, e.g. surface band bending and superimposed impurity absorption. We have at present no full microscopic understanding of the local damping function in the given sample $\gamma_0(\omega)$, but in Sec. IV B (see Fig. 10) we show that in an ideal crystal even at low carrier densities of the order of (10^{12} cm^{-3}) there is an appreciable and frequency-dependent dephasing of excitons.

IV. NONLINEAR BEHAVIOR OF PHASE JUMPS WITH INCREASING EXCITATION

A. Experimental results

In this section the experimental behavior of phase and amplitude of the transmitted electric field is investigated as a function of incident laser fluence. The latter is assumed to create steady quasiequilibrium carrier densities in the sample, at least for the short duration of the analysis, which focuses on data in the time interval 1–8 ps after pulse injection.

Results for intensity and phase are presented in Fig. 6.

The intensity shows the expected behavior: With increasing excitation the interferences between $1s$ and $2s$ excitons disappear, since the $2s$ exciton is damped out and vanishes in the shrinking band edge. Furthermore the decay times become shorter corresponding to an increase of the excitonic linewidth. The strong decrease of the intensity for the 13.4 W/cm^2 pulse at 2.3 ps can be understood in connection with the behavior of the phase shifts. With increasing excitation the signs of the observed phase shifts change. For laser power densities approaching 1 W/cm^2 the phase shift at 4.3 ps first becomes steeper, then changes sign, and finally becomes smoother again. At laser fluence 13.6 W/cm^2 the phase shift at 2.3 ps flips. Near these flips the phase becomes very steplike and the intensity strongly decreases. The latter will be demonstrated in Sec. IV C more in detail by the theoretical calculations (see Figs. 14 and 15).

As explained above, this characteristic behavior cannot be modeled with an additional Lorentzian broadening. Symmetric Lorentzian line shapes always lead to *positive* jumps of the phase. Even if the damping γ_n of the exciton series (3) is increased in such a way that an apparent asymmetry of the $1s$ resonance is introduced by broadening of higher-lying exciton states, the sequential order of the phase flips cannot be reproduced: In the experiment the phase shift at 4.3 ps changes its sign first, then the shift at 2.3 ps follows. This would be contrary if a Lorentzian broadening is used.

In Sec. III we have demonstrated that the sign of the phase jumps can be understood by considering (i) the interference of two oscillators and (ii) the relation between their amplitudes. To give a qualitative explanation of the density-dependent behavior of the phase shifts (see Fig. 6) we model the $1s$ exciton resonance by an asymmetric dielectric function

$$\epsilon(\omega) = \epsilon_b \left[1 + \frac{f_1}{\omega_1^2 - \omega^2 - 2i\gamma_1\omega} + \frac{f_2}{\omega_2^2 - \omega^2 - 2i\gamma_2\omega} \right], \quad (6)$$

consisting of two Lorentzians with energetic separation comparable with their damping. Taking the resonance frequencies arbitrarily as $\omega_{1,2} = 1.515 \text{ eV} \pm \Delta\omega/2$, the damping as $\gamma_2 = 2\gamma_1$ and the longitudinal transversal splittings as $f_1 = f_2 = f_0/2$ ($f_0 = 86 \text{ } \mu\text{eV}$ for the $1s$ exciton in GaAs) one simulates the phase curves shown in (see Fig. 7; for parameters γ_1 and $\Delta\omega$ see the inset, the dielectric background for GaAs is $\epsilon_b = 12.55$). Increasing the asymmetry leads to phase flips: first the phase jumps steepen, then they flip sign and eventually become smoother. This happens first for phase shifts at later times. Phase shifts at earlier times follow increasing density. From the behavior of the measured phase one can deduce that the excitation-induced dephasing leads to an asymmetric broadening of the exciton resonance with more weight on the high-energy side. Such an asymmetry is ubiquitous in excitonic spectra and has been reported earlier for higher excitation and larger initial broadening.⁴² It is important to note that the densities reported here are much smaller than the Mott density.

We performed pump and probe measurements with systematic variations of the spectrum and the time delay of the

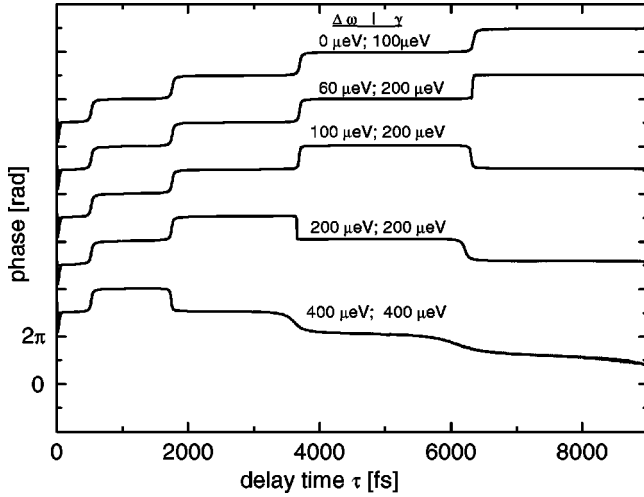


FIG. 7. Phase signals of a two oscillator model: depending on the degree of asymmetry (see the energetic separation $\Delta\omega$) phase jumps change sign.

pump pulse with respect to the probe pulse ($\tau_{delay}=0-20$ ps), and we found that the behavior of the phase jumps in the probe spectrum depended predominantly on the excitation intensity of the pump, as long as it created electron-hole pairs in the continuum. From this we conclude (i) that the propagation effects generated by the interfering polaritons in the picosecond time domain are dominated by a carrier system in quasi-equilibrium, i.e., time-independent system on the 10 ps scale, and (ii) that the dielectric function can be modeled within linear response theory.

B. Many-body theory of the excitonic absorption

In this section we present the basic ideas of a many-body description of the linear response of an excited semiconductor, which—in contrast to earlier treatments—is able to explain the asymmetric line shape of the exciton resonance discussed above. The nonlinear optical properties of a semiconductor induced by an intense laser pulse can be calculated by solution of the semiconductor Bloch equations (for a review see Ref. 19) that describe the dynamics of the coherent polarization $p_k(t)$ induced by the laser field, and the populations $f_k^{e,h}(t)$ of excited electrons (holes). The equation for the polarization reads

$$\left\{ i \frac{d}{dt} - \epsilon_k^e + \epsilon_k^h \right\} p_k(t) + N_k \Omega_k(t) = \frac{dp_k(t)}{dt} \Big|_{coll}, \quad (7)$$

The Hartree-Fock (HF) renormalized Rabi energy of the pulse

$$\Omega_k(t) = dE(t) + \sum_q v_{k-q} p_q(t) \quad (8)$$

and HF renormalized carrier energies

$$\epsilon_k^a = e_k^a - \Delta e_k^{a, HF} = e_k^a - \sum_q v_{k-q} f_q^a \quad (9)$$

are caused by Coulomb correlations; v_k is the bare Coulomb potential, and $N_k = 1 - f_k^e - f_k^h$ denotes the Pauli blocking. The characteristic many-particle effects beyond the HF renormalizations in Eqs. (8) and (9) are contained in the scattering integral on the right-hand side of Eq. (7). Within Green's function (GF) techniques it can be presented by^{43,44}

$$\frac{dp_k(t)}{dt} \Big|_{coll} = \int_{-\infty}^t dt' \{ \sum_{c\mu,k} \langle G_{c\mu,k}^<(t, t') \rangle G_{\mu\nu,k}^>(t', t) + G_{c\mu,k}^>(t, t') \sum_{\mu\nu,k} \langle G_{\mu\nu,k}^<(t', t) \rangle - \langle \leftrightarrow \rangle \}, \quad (10)$$

where the sum over the band index μ has to be performed. The two-band GF matrix $G_{\mu\nu,k}^{\approx}(t, t')$ is connected with the two-band density matrix $f_{\mu\nu,k}(t)$ via

$$f_{\mu\nu,k}^{\approx}(t) = \lim_{t' \rightarrow t} G_{\mu\nu,k}^{\approx}(t, t') = \begin{cases} f_{\mu,k}(t), & \mu = \nu = (c, v) \\ 1 - f_{\mu,k}(t) & \mu = c, \nu = v. \\ \mp p_k(t), & \mu = c, \nu = v. \end{cases} \quad (11)$$

While the diagonal elements represent the carrier distributions within the conduction and valence (c and v) bands, the off-diagonal elements are the laser-induced polarization with $p_k(t) = f_{cv,k}^<(t) = [f_{vc,k}^<(t)]^*$.

The two-band self-energy matrix $\Sigma_{\mu\nu,k}^{\approx}(t, t')$ contains the whole manifold of many-body effects, being itself a functional of the two-band GF matrix again. Since this basic quantity $G_{\mu\nu,q}^{\approx}(t, t')$ in the scattering integral (10) depends on two times, Eq. (7) is not a closed set of equations for the two-band density matrix (11). In order to get closed equations one has to apply an appropriate ansatz to reduce $G_{\mu\nu,q}^{\approx}(t, t')$ to $f_{\mu\nu,q}^{\approx}(t)$. In this paper we use an ansatz introduced in Ref. 45 taking into account causality and extended in Ref. 46 for the two-band semiconductor known as the generalized Kadanoff-Baym (GKB) ansatz:

$$G_{\mu\nu,k}^{\approx}(t, t') = \sum_{\lambda} [G_{\mu\lambda,k}^r(t, t') f_{\lambda\nu,k}^{\approx}(t') - f_{\mu\lambda,k}^{\approx}(t) G_{\lambda\nu,k}^a(t, t')]. \quad (12)$$

Applying this ansatz within the scattering term (10) the two-band density matrix at time t depends on their behavior at earlier times $t' \leq t$, that is, memory effects are taken into account. This is beyond the often used Markovian limit, where the two-band density matrix in the scattering term is approximated by its value at time t . As will be demonstrated later, the consideration of memory effects is the essential point for our explanation of the behavior of the phase shift of transmitted pulses. According to the experimental findings the carriers can be considered to be in thermal quasiequilibrium and one can restrict theory to investigate only their linear response. In this case the diagonal GF's G_{cc} and G_{vv} depend only on the difference of the two times. The carrier distributions are Fermi functions with given chemical potential and temperature that are not affected by the much weaker probe pulse, and only the kinetic equation for the polarization has to be solved.

Introducing relative $t=(t_1-t'_1)$ and center $T=(t_1+t'_1)/2$ times and performing Fourier transformations $t\rightarrow\omega$ and $T\rightarrow\Omega$, we can rewrite the GKB ansatz as

$$G_{aa,k}^{\cong}(\omega)=\hat{G}_{aa,k}(\omega)\times\begin{cases} 1-f^a(\omega) \\ f^a(\omega) \end{cases} \quad (13)$$

$$G_{eh,k}^{\cong}(\omega,\Omega)=\pm\{G_{hh,k}^r(\Omega/2-\omega)+G_{ee,k}^r(\omega+\Omega/2)\}p_k(\Omega).$$

$\hat{G}_{aa,k}$ is the spectral function and $f^a(\omega)=1/[1+\exp[(\omega-\mu_a)/kT]]$ is the Fermi distribution of carriers⁴⁷ with the chemical potential μ_a and temperature T . Furthermore we changed from the two-band picture into the electron-hole picture with $a=e$ and h standing for electrons and holes, respectively. Terms with off-diagonal retarded and advanced GF's, which give rise to laser induced renormalizations^{48,49,46} in the sense of a linear response theory can be neglected. The spectral function of carriers $\hat{G}_{aa,k}(\omega)$, which is related to the imaginary part of the retarded GF, is used within the quasiparticle approximation (QPA),

$$\begin{aligned} \hat{G}_{aa,k}(\omega) &= -2 \operatorname{Im} G_{aa,k}^r(\omega), \\ G_{aa,k}^r(\omega) &= 1/[\omega - \varepsilon_k^a + i\Gamma_k^a/2], \end{aligned} \quad (14)$$

where $\varepsilon_k^a = e_k^a - \Delta_k^{a,\text{HF}} - \operatorname{Re} \Sigma_{aa,k}^r(\varepsilon_k^a)$ is the renormalized carrier energy and $\Gamma_k^a = -2 \operatorname{Im} \Sigma_{aa,k}^r(\varepsilon_k^a)$ the damping (inverse lifetime of a carrier within state ε_k^a). Both are determined by the real and imaginary part of the retarded carrier self-energy $\Sigma_{aa,k}^r(\omega)$ taken at the renormalized carrier dispersion $\omega = \varepsilon_k^a$. Throughout this paper we use the self-energies within the random phase approximation (RPA):

$$\Sigma_{aa,k}^{\cong}(\omega) = \sum_q \int \frac{d\omega'}{2\pi} G_{aa,k-q}^{\cong}(\omega - \omega') V_q^{\cong}(\omega'), \quad (15)$$

$$\Sigma_{eh,k}^{\cong}(\omega,\Omega) = \sum_q \int \frac{d\omega'}{2\pi} G_{eh,k-q}^{\cong}(\omega - \omega', \Omega) V_q^{\cong}(\omega').$$

The question whether the RPA is valid is strongly connected with the existence of an excitonic population in the sample. Even though the experiments were performed at a lattice temperature of 2 K, we have to model in the theoretical calculations the temperature of photoexcited carriers. Since our 40 fs pulses were centered above the band edge (1.525 eV, 6 meV above the band edge), the carriers get a considerable excess energy, which is much larger than a thermal energy corresponding to 2 K. A temperature of 30 K used in the calculations corresponds to an thermal energy of 2.5 meV, providing the best agreement with the experiment. In the low-temperature regime considered here there is no scattering mechanism, which cools down the carriers within several picoseconds to the bath temperature of 2 K. Otherwise, an estimation of the density of bound e - h pairs in a thermal plasma via a mass-action law predicts excitonic populations to become relevant below 15 K. At last we have no exact

measure of the temperature of the photoexcited carriers, but it is safe to assume that we are above the limit where a population of excitons becomes important.

On one hand the self-energies $\Sigma_{aa,k}^{\cong}(\omega)$ enter the scattering term (10) of the SBE (7) and play the role of scattering rates. On the other hand, the retarded carrier self-energy

$$\begin{aligned} \Sigma_{aa,k}^r(\omega) &= \int \frac{d\omega'}{2\pi} \frac{\Gamma_k^a}{\omega - \omega' + i\varepsilon}, \quad \Gamma_k^a = \Sigma_{aa,k}^>(\varepsilon_k^a) \\ &\quad + \Sigma_{aa,k}^<(\varepsilon_k^a), \end{aligned} \quad (16)$$

characterizes the carrier spectral function (14), and via the GKB ansatz (13) it determines the GF's in Eq. (15). Within the QPA it can be written as

$$\begin{aligned} \Sigma_{aa,k}^{r,\text{QPA}} &= \Sigma_{aa,k}^r(\varepsilon_k^a) \\ &= \sum_q \int \frac{d\omega}{2\pi} \frac{[1-f_q^a]V_{k-q}^>(\omega) + f_q^a V_{k-q}^<(\omega)}{\varepsilon_k^a - \varepsilon_q^a - \omega + i\Gamma_q^a/2}. \end{aligned} \quad (17)$$

In this way the carrier self-energies and GF's have to be determined self-consistently by numerically iterating Eqs. (13)–(16). This is well known from GF's theory;⁴⁷ however, mostly a simple δ -function-like spectral function $\hat{G}_{aa,k}(\omega) = 2\pi \delta(\omega - e_k^a)$ was used to calculate the carrier self-energies (15). The influence of the Lorentzian-like broadened carrier spectral function in comparison to a δ -function-like on the properties of the exciton will be discussed below in more detail.

First we introduce the GKB ansatz (13) and the RPA self-energies (15) into the scattering term (10) of the equation for the polarization (7). After Fourier transformation it can be rewritten as

$$\begin{aligned} \{\omega - \varepsilon_k^e - \varepsilon_k^h - \Sigma_k^r(\omega)\} p_k(\omega) \\ + \sum_q \{N_k v_{k-q} + \Theta_{k,q}(\omega)\} p_q(\omega) = N_k dE(\omega). \end{aligned} \quad (18)$$

The non-Markovian character of the polarization dynamics is now reflected in the ω dependence of the complex interaction matrix

$$\begin{aligned} \Theta_{k,q}(\omega) &= \Delta V_{k,q}^{eff}(\omega) - i\Gamma_{k,q}(\omega) \\ &= \sum_{a \neq b} \int \frac{d\bar{\omega}}{2\pi} \frac{[1-f_k^a]V_{k-q}^>(\bar{\omega}) + f_k^a V_{k-q}^<(\bar{\omega})}{\omega - \varepsilon_k^a - \varepsilon_q^b - \bar{\omega} + i[\Gamma_k^a + \Gamma_q^b]/2} \end{aligned} \quad (19)$$

and of the retarded interband self-energy

$$\Sigma_k^r(\omega) = \sum_q \Theta_{q,k}(\omega) = \Delta e_k^{sc}(\omega) - i\Gamma_k(\omega). \quad (20)$$

Both describe many-body effects beyond the Coulomb-HF renormalizations (8) and (9), while the real part of the inter-

band self-energy $\Delta e_k^{\text{sc}}(\omega)$ gives rise to a renormalization of the interband energy, the imaginary part $\Gamma_k(\omega)$ represents the (diagonal) dephasing. The real part $\Delta V_{k,q}^{\text{eff}}(\omega)$ of the complex matrix $\Theta_{q,k}(\omega)$ describes the renormalization of the Coulomb interaction due to many-body effects in Eq. (18), and the imaginary part $\Gamma_{k,q}(\omega)$ is the so-called off-diagonal dephasing.

The GF of the screened potential (plasmon GF)

$$V_q^{\approx}(\omega) = n^{\approx}(\omega) \hat{V}_q(\omega), \quad \hat{V}_q(\omega) = \text{Im}\{\varepsilon^{-1}(q, \omega)\}, \quad (21)$$

is related to the imaginary part of the inverse longitudinal dielectric function $\varepsilon(q, \omega)$ describing the spectral properties of plasmons. Throughout this paper we use a RPA dielectric function that takes finite damping of carrier states into consideration. For a more detailed discussion of dynamical screening we refer to an earlier paper.³² The plasmon distribution is given for thermal equilibrium by a Bose function

$$n(\omega) = 1/[1 - \exp(\hbar\omega/kT)], \quad (22)$$

$$n^{<}(\omega) = n(\omega), \quad n^{>}(\omega) = 1 + n(\omega).$$

As a consequence of the non-Markovian character of the scattering integrals the many-body effects depend on the frequency ω of the laser pulse. A clear physical interpretation of this frequency dependence can be given by considering the plasmon-pole approximation for the inverse dielectric function

$$\text{Im}[\varepsilon^{-1}(q, \omega)] = \frac{\pi\omega_{pl}^2}{2\omega_q} [\delta(\omega + \omega_q) - \delta(\omega - \omega_q)], \quad (23)$$

where the plasmon dispersion ω_q is determined by the plasma frequency ω_{pl} and the inverse screening length κ :

$$\omega_q^2 = \omega_{pl}^2(1 + q^2/\kappa^2) + (\hbar^2 q^2/4\mu)^2, \quad (24)$$

$$\omega_{pl}^2 = 16\pi E_{ex}^b a_{ex}^3, \quad \kappa^2 = -\sum_{a,q} \frac{\partial f_q^a}{\partial e_q^a}.$$

With the δ -function-like spectral functions in Eq. (23) the interaction matrix can be reduced to

$$\Theta_{k,k-q}(\omega) = \frac{\pi\omega_{pl}^2}{2\omega_q} \sum_{a \neq b} \left\{ \frac{[1 - f_k^a][1 + n(\omega_q)] + f_k^a n(\omega_q)}{\omega - \epsilon_k^a - \epsilon_{k-q}^b - \omega_q + i\varepsilon} - [\omega_q \rightarrow -\omega_q] \right\}. \quad (25)$$

Considering the energy transfer relation in the denominator of the complex interaction matrix (25) the underlying scattering process can be understood as the generation of an electron-hole pair with the energy $\epsilon_k^a + \epsilon_{k-q}^b$ due to a laser photon of the energy ω accompanied by emission or absorption (second term with $\omega_q \rightarrow -\omega_q$) of a plasmon with energy ω_q . Using the RPA dielectric function in contrast to the plasmon-pole approximation (23) the spectral function of

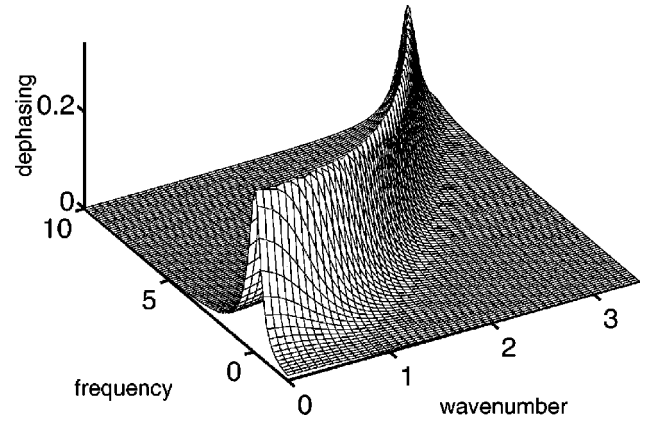


FIG. 8. Dephasing $\Gamma_k(\omega)$ [E_{ex}^b] in dependence on energy ($\omega - E_{\text{gap}}/E_{ex}^b$) and wavenumber ka_{ex} (a_{ex} is the excitonic Bohr radius) for a carrier density of $n = 1 \times 10^{14} \text{ cm}^{-3}$. The carrier damping $\Gamma_k^a(\omega)$ was determined self-consistently by iteration of Eqs. (13)–(16).

plasmons is broadened by Landau damping and the plasmon dispersion is limited by the pair continuum.^{19,50,51,32}

Our consideration of frequency dependent many-body effects goes beyond earlier treatments (see, for instance, Refs. 29 and 31 and the literature cited therein), where in accordance with the energy conservation relation, the Boltzmann collision term of the kinetic equation for the carrier distributions $\bar{\omega} - \epsilon_k^a + \epsilon_q^a$ was used. The formal problems in deriving such a collision term were already mentioned in Ref. 44. There is no systematic way to justify such energy conservation relation for the scattering term in the equation for the polarization. However, the use of such a scattering term simplifies the solution of Eq. (18) considerably, since it is independent of the laser frequency ω and has to be calculated only once for the whole spectrum. In this case the interaction matrix is given by

$$\Theta_{k,q}^{\text{QPA}} = \sum_a \int \frac{d\omega}{2\pi} \frac{[1 - f_k^a]V_{k-q}^{>}(\omega) + f_k^a V_{k-q}^{<}(\omega)}{\varepsilon_k^a - \varepsilon_q^a - \omega + i[\Gamma_k^a + \Gamma_q^a]/2}. \quad (26)$$

If the carrier damping Γ_k^a is neglected, the retarded interband self-energy $\Sigma_k^{\text{QPA}} = \sum_q \Theta_{q,k}^{\text{QPA}}$ is simply the sum over the carrier self-energies (17). Considering the imaginary part of the interband self-energy to be the dephasing rate, one finds the corresponding dephasing time $T_2 = \hbar/\Gamma^{\text{QPA}}$ to be simply related to the relaxation times T_1^h of the carriers via $1/T_2 = 1/T_1^e + 1/T_1^h$.

However, this relation is strongly different in our approach: First of all the dephasing rate strongly depends on the frequency ω . This is demonstrated in Fig. 8, where $\Gamma_k(\omega)$, introduced in Eq. (20), is plotted for a carrier density of $n = 1 \times 10^{14} \text{ cm}^{-3}$ and a temperature of $T = 30 \text{ K}$. In the considered frequency region the maximum value of the dephasing follows the renormalized interband dispersion $\omega = \epsilon_k^e + \epsilon_k^h$. Within the QPA (26) the dephasing only depends on the wave number, and for $k=0$ it agrees with the frequency dependent dephasing (20) at $\omega=0$ (band gap).

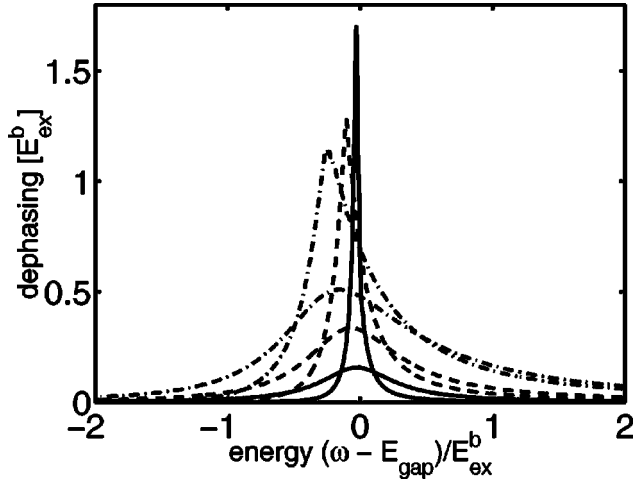


FIG. 9. Dephasing $\Gamma_k(\omega)$ as function of the frequency ω for $k=0$ and different carrier densities: $n=1 \times 10^{13} \text{ cm}^{-3}$ (full lines), $n=1 \times 10^{14} \text{ cm}^{-3}$ (dashed), $n=5 \times 10^{14} \text{ cm}^{-3}$ (dash-dotted). Upper curves correspond to $\Gamma_0=0.01$ and lower curves to $\Gamma_0=0.3$ (see text).

Moreover, the magnitude of the dephasing strongly depends on the carrier damping Γ_k^a (14), which enters the denominator of the interaction matrix. To demonstrate this we have fixed the sum $\Gamma_k^a + \Gamma_q^b$ in Eq. (19) by a constant $\bar{\Gamma}$. The result for the dephasing in dependence on the frequency in the vicinity between the exciton and the band gap is shown in Fig. 9 for $\bar{\Gamma}=0.01$ and 0.3 and three different carrier densities. For better clarity we have restricted here to the case $k=0$. The maximum dephasing appearing at the renormalized band gap strongly increases if $\bar{\Gamma}$ is decreased. Note that this maximum value corresponds to the QPA (26) and is valid within this approximation for the whole frequency domain ranging from the 1s exciton high up into the continuum. This is completely different within our approach: Towards the exciton (around $\omega=-1$, excitonic units are used) and higher in the bands the dephasing strongly decreases. Quite generally, the consideration of a finite carrier damping is beyond earlier treatments, where the dephasing was calculated within QPA (26) (Refs. 51, 50, and 32) or with the interaction matrix (19) (Refs. 25 and 52) using additionally a δ -function-like spectral function instead of Eq. (14). This corresponds to the limit $\bar{\Gamma} \rightarrow 0$ and the results are nearly the same as those for the lowest $\bar{\Gamma}$ in Fig. 9. In Ref. 31 the influence of phenomenologically introduced quasiparticle damping $\bar{\Gamma}$ on the interband self-energy was investigated at higher excitation in ZnSe, where gain appears. Using the QPA (26) and static approximation for the screened potential, the influence of the quasiparticle damping was not as pronounced as for the lower excitation considered here. Considering higher carrier densities in our approach the influence of a quasiparticle carrier damping becomes lower too.

There is still another inconsistency in the behavior of the dephasing presented in Fig. 9: If the carrier density is increased for a constant quasiparticle carrier damping $\bar{\Gamma}$ the maximum dephasing at the renormalized band gap decreases.

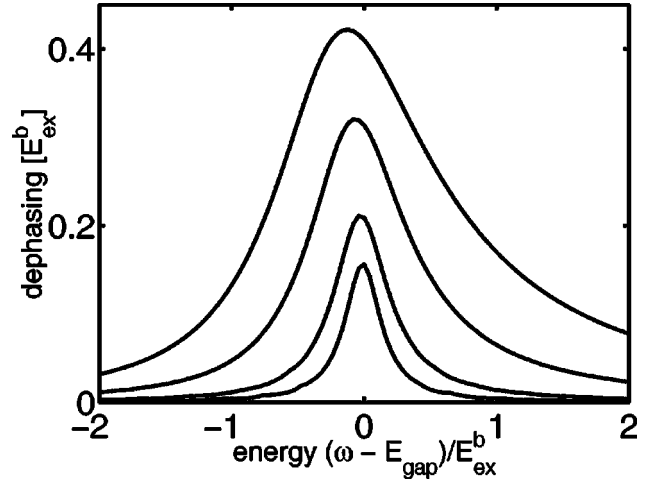


FIG. 10. Dephasing $\Gamma_k(\omega)$ as a function of frequency ω for $k=0$ and for different carrier densities from below to above: $n=1 \times 10^{12} \text{ cm}^{-3}$, $n=1 \times 10^{13} \text{ cm}^{-3}$, $n=1 \times 10^{14} \text{ cm}^{-3}$, $n=1 \times 10^{15} \text{ cm}^{-3}$, $n=5 \times 10^{14} \text{ cm}^{-3}$.

In Fig. 10 the dephasing is presented as a function of frequency in the vicinity between the exciton and the band gap for different carrier densities. In contrast to Fig. 9 the carrier damping was calculated iterating Eqs. (13)–(16). We find a qualitatively similar behavior of the dephasing as in Fig. 9: a maximum at the renormalized band gap and a decrease towards the exciton and higher into the bands. In contrast to Fig. 9, the dephasing increases within the whole frequency region from below the exciton to above the band gap if the carrier density is increased. The peak value of the dephasing corresponds roughly to the sum of the carrier damping $\Gamma_0^e + \Gamma_0^h$ taken at $k=0$ (there is only a weak decrease at the dispersion if k is increased).

In Ref. 37 good agreement of the approach³⁶ with the experiment could be achieved, explaining the temporal evolution of four-wave-mixing signals without taking into account the damping of carrier states. However, in contrast to our considered situation (low temperatures and excitonic properties), an excitation 50 meV above the band edge at room temperature and densities between 10^{15} and 10^{18} cm^{-3} were investigated. With increasing temperature the dephasing presented in Fig. 10, which includes the carrier damping, becomes broader, the wings become more flat, and the dependence on the energy weaker. This behavior is still enhanced with increasing carrier densities, where additionally the influence of a finite carrier damping becomes small (see discussion above).

How will the sensitive dependence of dephasing on density be reflected in the excitonic absorption? With consideration of the linear response, the susceptibility is simply related to the coherent polarization via

$$p(\omega) = \sum_k p_k(\omega) = \chi(\omega) E(\omega). \quad (27)$$

First we have to reproduce the behavior of the transmitted pulses at low excitation. Starting with a constant dephasing, which describes the linewidth of the exciton at low excita-

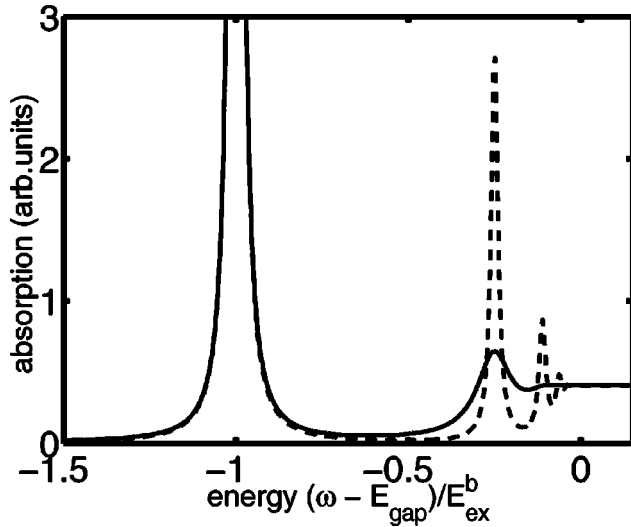


FIG. 11. Absorption of the unexcited sample with a constant dephasing $\Gamma=40 \mu \text{ eV}$ (dashed line) and a frequency dependent background dephasing $\gamma_0(\omega)$ modeling the experimental results (full).

tion, and neglecting all carrier-induced renormalizations ($f_k^e, f_k^h \rightarrow 0$), our solution of the SBE (18) for the imaginary part of the susceptibility $\chi(\omega)$ is presented in Fig. 11. The ground state of the exciton ($1s$ state) and the excited states are clearly resolved. Our result exactly corresponds to that of the broadened Elliot formula.³⁹ We have already discussed in Sec. III that the pulse propagation experiments have shown that the nominal linewidths of the individual exciton states ($n=1,2,\dots$) increase with increasing quantum number n even at low excitation and there is only a relatively weak influence of the higher exciton states on phase and amplitude of the transmitted pulses. The imaginary part of the susceptibility including the $\gamma_0(\omega)$ according to Eq. (5) is plotted in Fig. 11 for comparison. The influence of higher exciton states is strongly reduced, only the $2s$ state is still resolved.

There is still a problem in calculating the real part of the susceptibility, since the sum over k in Eq. (27) diverges for the unexcited case ($f_k^e, f_k^h \rightarrow 0$), while the carrier-induced

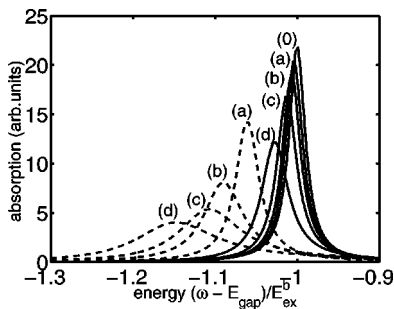


FIG. 12. Absorption in the vicinity of the $1s$ exciton in dependence on the detuning with respect to the band gap for different carrier densities: (0) $n=0$, (a) $n=5 \times 10^{13} \text{ cm}^{-3}$, (b) $n=1 \times 10^{14} \text{ cm}^{-3}$, (c) $n=2 \times 10^{14} \text{ cm}^{-3}$, (d) $n=5 \times 10^{14} \text{ cm}^{-3}$; (full lines): many-body effects according to Eq. (19); dashed lines: within QPA (26).

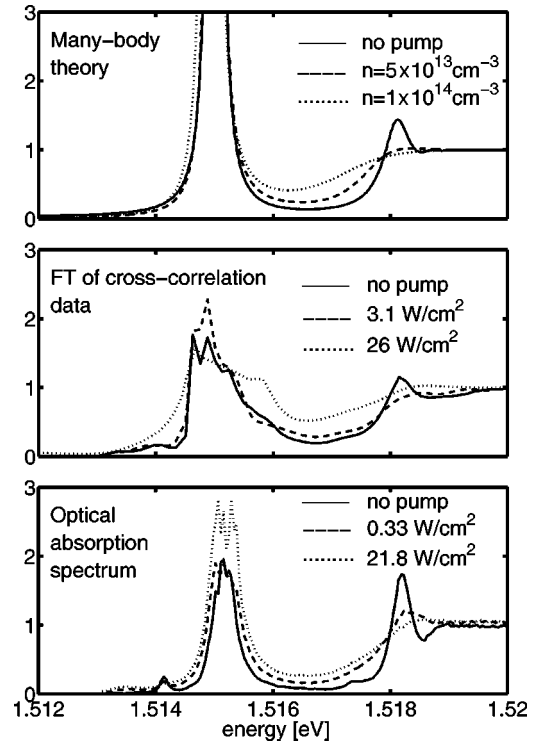


FIG. 13. Comparison of theoretical edge spectra (top) with experimental data from Fourier-transformed interferometric measurements (center) and direct optical absorption taken with a grating spectrometer and a cw 2.18 eV pump (bottom). All curves are normalized to 1 at the band edge. Three different levels of excitation are shown in each case.

contribution behaves properly. Therefore only the imaginary part of the susceptibility can be determined solving the SBE (18). For the nonexcited semiconductor the result of the broadened Elliot formula can be used for the real part of the susceptibility $\chi^{n=0}(\omega)$. For the excited semiconductor the real part of $\chi(\omega)$ is determined in the following way: By subtracting the imaginary part $\chi_k^{n=0}(\omega)$ from that imaginary part resulting from the solution of the SBE, the divergency is omitted. So the sum over k and a Kramers-Kronig transformation can be performed to get the carrier-induced contribution of the real part of $\chi(\omega)$. Finally the contribution of the nonexcited semiconductor has to be added.

In order to describe the influence of many-body effects with increasing excitation (carrier density) we have solved the SBE (18) with the interaction matrix (19) and with the self-consistently determined carrier self-energies as we have demonstrated particularly in Fig. 10 for the diagonal dephasing. To fit the experiments at low excitation we have added the background damping $\gamma_0(\omega)$ to the diagonal (carrier induced) dephasing. In Fig. 12 the imaginary part of the susceptibility (absorption) is shown for different carrier densities. Results with the QPA are presented for comparison with dotted lines, showing an enhanced redshift and broadening of the exciton. This is due to the nature of this approximation, which overestimates the interband self-energy (both dephasing and energy renormalization) using, e.g., the maximum value of the dephasing at the band gap for the whole spectral

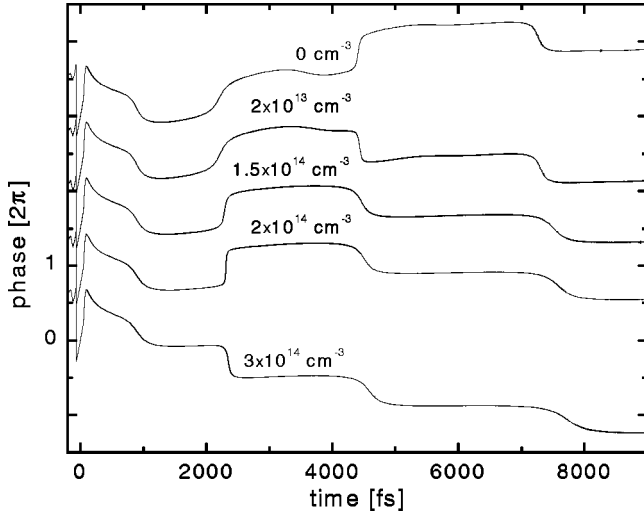


FIG. 14. Phase of transmitted pulses calculated for different carrier densities with the susceptibility presented in Fig. 12.

region. The $2s$ state of the exciton is not displayed, since it plays only a minor role for the pulse transmission, at the lowest density $n = 5 \times 10^{13} \text{ cm}^{-3}$ it is already bleached out. Furthermore, due to the consideration of a finite quasiparticle carrier damping in the interaction matrix, the shift of the exciton is reduced in comparison to earlier treatments,^{25,52} where it was neglected. The asymmetry of the excitonic line shape increasing up with increasing carrier density is only weak, but is strong enough to be responsible for the observed nonlinear behavior of the phases of transmitted pulses.

C. Comparison between theory and experiment

In Fig. 13 we compare our theoretical results of the absorption spectrum for three different carrier densities (top) with the corresponding Fourier transformed cross-correlation data of measured interferograms in the one-beam configuration (center) and also with absorption spectra obtained directly in the frequency domain with an incandescent light

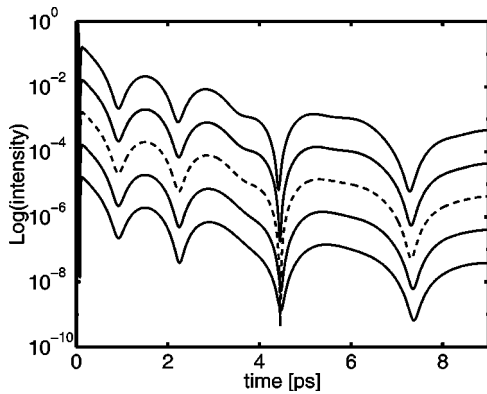


FIG. 15. Behavior of the intensity of transmitted pulses (normalized), calculated for four carrier densities around the density corresponding to the phase flip at $\tau = 4.3$ ps. From above to below: $n = 0$, $n = 5 \times 10^{12} \text{ cm}^{-3}$, $n = 1 \times 10^{13} \text{ cm}^{-3}$ (dashed line), $n = 2 \times 10^{13} \text{ cm}^{-3}$, $n = 3 \times 10^{13} \text{ cm}^{-3}$, where an offset of 10 between different curves was used.

source and a conventional grating spectrometer, and 2.18 eV cw laser pumping (bottom), both taken on the same sample spot at lattice temperature $T = 2$ K. For comparison the data were normalized to give the relative absorption strength one at the band edge. The three data sets for the linear case (i.e., no pump pulse, no screening carriers) can be compared directly, while the sets for increasing excitation are labeled by the carrier density (theory, top) and the pump power density in experiment (center, bottom).

In order to avoid windowing effects in the Fourier transformation of the interferograms we had to extrapolate the experimental data for delay times larger than 8 ps. Beyond this value the fringe modulation could no longer be measured due to the limited dynamical range of the interferometric setup: after 8 ps the intensity of the $1s$ free polarization decay has dropped more than four orders compared with its maximum at time zero. The comparison of three independent data sets in Fig. 13 shows that with increasing excitation the bleaching of the $2s$ -exciton state and the characteristic increase of absorption strength between the $1s$ - and the $2s$ -exciton energies shows very good agreement between theory and experiment.

Our theoretical results for the susceptibility are now used instead of the oscillator model (6) to describe amplitude and phase of transmitted pulses. In Fig. 14 the phase is presented for different carrier densities and a temperature of 30 K. With increasing carrier density the phase flips at the single polariton beat nodes change their direction. In agreement with the experiments, the phase jump at 4.3 ps flips down first. This happens already at a very low carrier density between $1 \times 10^{13} \text{ cm}^{-3}$ and $2 \times 10^{13} \text{ cm}^{-3}$ (compare Fig. 6). The phase jump at 2.3 ps follows for carrier densities between 2×10^{14} and $3 \times 10^{14} \text{ cm}^{-3}$. In agreement with the experiments we find that the flips become nearly steplike in the vicinity of the beat nodes: here they change their sign and become smoother if the corresponding carrier density (fluence of the pulse) is increased or decreased (compare Fig. 4, where the beat phenomenon between two oscillators was demonstrated).

Performing our calculations we checked the influence of the temperature on the absorption in a range between 20 and 77 K. The main result is that the order of the phase flips remained unchanged, only the carrier densities, where the flips appear, change. For 30 K we found the best agreement of our results with the experiments.

The intensity of the transmitted pulses shows a characteristic behavior as well: at densities where the phase jump changes sign the intensity at the beat node becomes a minimum (see dashed line in Fig. 14). The phase jump changes sign if the density n^{flip} is slightly above $n = 1 \times 10^{13} \text{ cm}^{-3}$ (compare with Fig. 13). This can be understood in terms of the model for the beating between two oscillators discussed above [see (4) and Fig. 4]: At the phase flip the interfering polariton wave packets more or less cancel, their amplitudes are nearly equal. If the carrier density is below (above) n^{flip} one of the amplitudes is greater (smaller) than the other, and this leads to the change of sign of the phase flip.

Very similar behavior is found in the experiments (see Fig. 6). But due to noise and the limited precision of the

measurements it is somewhat less pronounced than in the calculations. The $2s$ -exciton state is already bleached out at very low carrier densities (fluences of the laser pulses). This can be observed in the absorption spectra as well as in the intensity of the transmitted pulses (see $n = 3 \times 10^{13} \text{ cm}^{-3}$ in Fig. 15). The carrier densities chosen for the theory plots correspond roughly to those that can be estimated from the laser fluence and the beam profile of the pulses in experiment (see Figs. 2 and 6). The ratio of the carrier densities in our calculations, where the two carrier-induced phase flips appear, agrees well with the corresponding ratio of laser powers in the experiments. In particular the low carrier density and low laser power for which the phase shift at 4.3 ps changes its sign demonstrate the good agreement between experiment and theory.

The determination of absolute e - h pair densities in experiments with uncladded samples is a formidable problem. In general, surface recombination and other loss channels for excitons are not well characterized. This limits severely the accuracy of assumptions and only a crude estimate of optically generated carrier densities is possible for each given experimental laser fluence. Therefore we do not compare directly our experimental results with the theoretical calculations in one figure. The central message of our paper, however, is the quantitative explanation of the behavior of the phase signals for a wide range of pair densities, and particularly the prediction of the order of the flips in terms of many-body effects in the excited carrier system. Simple treatments with symmetrically broadened Lorentzian oscillators inserted into the Elliot formula fail here.

V. SUMMARY

In summary we have reported on detailed amplitude and phase measurements of polariton pulse propagation as a function of excitation density in bulk GaAs at low temperature. We have observed a characteristic excitation dependent change of the phase of the transmitted electric field at the polariton propagation beat nodes. In contrast to the limit of low excitation, where the phase jumps are characterized by $+\pi$, the flips change their sign from $+\pi$ to $-\pi$ in a certain order with increasing excitation density. This phase behavior can be related to the increase of an excitation induced asymmetry of the $1s$ exciton resonance at its high-energy side. All details of the measured excitonic line shapes could be described theoretically including frequency-resolved many-body effects. Energy renormalization and dephasing give rise to such asymmetric excitonic line shapes and explain the correct order of the changes of the phase shifts. The frequency dependence of the many-body effects results here from the inclusion of non-Markovian memory effects in the scattering term of the semiconductor Bloch equations.

ACKNOWLEDGMENTS

The theoretical part of this work was supported by the Deutsche Forschungsgemeinschaft through the Schwerpunktprogramm ‘‘Quantenkohärenz in Halbleitern’’ and the experimental part through the Sonderforschungsbereich 345 in Göttingen.

*Electronic address: manzke@physik3.uni-rostock.de

¹A. Stahl and I. Balslev, *Electrodynamics of the Semiconductor Band Edge*, Springer Tracts Modern Physics (Springer, Berlin, 1987), Vol. 110.

²J. J. Hopfield, Phys. Rev. **182**, 945 (1969).

³S. J. Pekar, Fiz. Tverd. Tela (Leningrad) **33**, 1022 (1958) [Sov. Phys. Solid State **4**, 953 (1962)].

⁴*Proceedings of the First Taormina Conference on the Structure of Matter*, Taormina, Italy, 1972, edited by E. Burstein and F. de Martini (Pergamon, London, 1974).

⁵C. Weisbuch and R. G. Ulbrich, *Topics in Applied Physics* (Springer, Berlin, 1982), Vol. 51.

⁶C. Andreani, in *Confined Electrons and Photons*, edited by E. Burstein and C. Weisbuch, NATO ASI Series B (Plenum, London, 1995), Vol. 340, p. 57.

⁷V. A. Kiselev, I. V. Makarenko and I. N. Uraltsev, Phys. Status Solidi B **98**, 773 (1980).

⁸R. G. Ulbrich and G. W. Fehrenbach, Phys. Rev. Lett. **43**, 963 (1979).

⁹K. Ema and M. Kuwata-Gonokami, Phys. Rev. Lett. **75**, 224 (1995).

¹⁰D. Fröhlich, A. Kulik, B. Uebbing, A. Mysyrowicz, V. Langer, H. Stolz, and W. von der Osten, Phys. Rev. Lett. **67**, 2343 (1991).

¹¹S. Nüsse, P. Haring Bolivar, H. Kurz, F. Levy, A. Chevy, and O. Lang, Phys. Rev. B **55**, 4620 (1997).

¹²U. Neukirch and K. Wundke, Phys. Rev. B **55**, 15 408 (1997).

¹³A. Knorr, R. Binder, M. Lindberg, and S. W. Koch, Phys. Rev. A **46**, 7179 (1992).

¹⁴J. Tignon, T. Hasche, D. S. Chemla, H. C. Schneider, F. Jahnke, and S. W. Koch, Phys. Rev. Lett. **84**, 3382 (2000).

¹⁵H. Giessen, A. Knorr, S. Haas, S. W. Koch, S. Linden, J. Kuhl, M. Hetterich, M. Grun, and C. Klingshirn, Phys. Rev. Lett. **81**, 4260 (1998).

¹⁶G. W. Fehrenbach, W. Schäfer, J. Treusch, and R. G. Ulbrich, Phys. Rev. Lett. **49**, 1281 (1982).

¹⁷R. Zimmermann, K. Kilimann, W. D. Kraeft, D. Kremp, and G. Röpke, Phys. Status Solidi B **90**, 175 (1978).

¹⁸C. Ell, R. Blank, S. Benner, and H. Haug, J. Opt. Soc. Am. B **6**, 2006 (1989).

¹⁹H. Haug and S. W. Koch, *Quantum Theory of the Optical and Electronic Properties of Semiconductors* (World Scientific, Singapore, 1990).

²⁰W. Schäfer, R. Binder, and K. H. Schuldt, Z. Phys. B: Condens. Matter **70**, 145 (1988).

²¹G. Böhne, T. Sure, R. G. Ulbrich, and W. Schäfer, Phys. Rev. B **41**, 7549 (1990).

²²S. Arndt, W. D. Kraeft, and J. Seidel, Phys. Status Solidi B **194**, 601 (1996).

²³M. Lindberg and S. W. Koch, Phys. Rev. B **38**, 3342 (1988).

²⁴G. Manzke, Q. Y. Peng, U. Moldzio, and K. Henneberger, Phys. Status Solidi B **206**, 37 (1998).

²⁵G. Manzke, Q. Y. Peng, K. Henneberger, U. Neukirch, K. Hauke, K. Wundke, J. Gutowski, and D. Hommel, Phys. Rev. Lett. **80**, 4943 (1998).

²⁶F. Rossi, S. Haas, and T. Kuhn, Phys. Rev. Lett. **72**, 152 (1994).

- ²⁷S. Hughes, A. Knorr, S. W. Koch, R. Binder, R. Indik, and J. V. Moloney, *Solid State Commun.* **100**, 555 (1996).
- ²⁸F. Jahnke, M. Kira, S. W. Koch, G. Khitrova, E. K. Lindmark, T. R. Nelson, Jr., D. V. Wick, J. D. Berger, O. Lyngnes, H. M. Gibbs, and K. Tai, *Phys. Rev. Lett.* **77**, 5257 (1996).
- ²⁹S. Haas, F. Rossi, and T. Kuhn, *Phys. Rev. B* **53**, 12 855 (1996).
- ³⁰F. Jahnke, M. Kira, and S. W. Koch, *Z. Phys. B: Condens. Matter* **104**, 559 (1997).
- ³¹A. Girndt, F. Jahnke, A. Knorr, S. W. Koch, and W. W. Chow, *Phys. Status Solidi B* **202**, 725 (1997).
- ³²G. Manzke, U. Moldzio, and K. Henneberger, *Phys. Status Solidi B* **202**, 961 (1997).
- ³³L. Banyai, D. B. Tran Thoai, E. Reitsamer, H. Haug, D. Steinbach, M. U. Wehner, M. Wegener, T. Marschner, and W. Stolz, *Phys. Rev. Lett.* **75**, 2188 (1995).
- ³⁴C. Fürst, A. Leitenstorfer, A. Laubereau, and R. Zimmermann, *Phys. Rev. Lett.* **78**, 3733 (1997).
- ³⁵M. U. Wehner, M. H. Ulm, D. S. Chemla, and M. Wegener, *Phys. Rev. Lett.* **80**, 1992 (1998).
- ³⁶L. Banyai, Q.T. Vu, B. Mieck, and H. Haug, *Phys. Rev. Lett.* **81**, 882 (1998).
- ³⁷W. A. Hügel, M. F. Heinrich, M. Wegener, Q. T. Vu, and L. Bányai, and H. Haug, *Phys. Rev. Lett.* **83**, 3313 (1999).
- ³⁸C. Sieh, T. Meier, F. Jahnke, A. Knorr, S. W. Koch, P. Brick, M. Hübner, C. Ell, J. Prineas, G. Khitrova, and H. M. Gibbs, *Phys. Rev. Lett.* **82**, 3112 (1999).
- ³⁹C. Tanguy, *Phys. Rev. Lett.* **75**, 4090 (1995).
- ⁴⁰C. Tanguy (private communication).
- ⁴¹U. Neukirch, K. Wundke, J. Gutowski, and D. Hommel, *Phys. Status Solidi B* **196**, 473 (1996).
- ⁴²G. W. Fehrenbach and R. G. Ulbrich, *J. Lumin.* **30**, 154 (1984).
- ⁴³H. Haug and C. Ell, *Phys. Rev. B* **46**, 2126 (1992).
- ⁴⁴R. Binder and S. W. Koch, *Prog. Quantum Electron.* **19**, 307 (1995).
- ⁴⁵P. Lipavski, V. Spicka, and B. Velicky, *Phys. Rev. B* **34**, 6933 (1986).
- ⁴⁶H. Haug, *Phys. Status Solidi B* **173**, 139 (1992).
- ⁴⁷L. P. Kadanoff and G. Baym, *Quantum Statistical Mechanics* (Benjamin, New York, 1962).
- ⁴⁸K. Henneberger and H. Haug, *Phys. Rev. B* **38**, 9759 (1988).
- ⁴⁹F. Jahnke and K. Henneberger, *Phys. Rev. B* **45**, 4077 (1992).
- ⁵⁰R. Binder, A. E. Paul, D. Scott, K. Henneberger, and S. W. Koch, *Phys. Rev. B* **45**, 1107 (1992).
- ⁵¹D. C. Scott, R. Binder, and S. W. Koch, *Phys. Rev. Lett.* **69**, 347 (1992).
- ⁵²J. S. Nägerl, B. Stabenau, G. Böhne, R. G. Ulbrich, G. Manzke, and K. Henneberger, *Phys. Status Solidi A* **178**, 559 (2000).